Three-Dimensional Dynamic Model of the Knee

Seonpil Kim*

(*Received December 17, 1997*)

A three-dimensional dynamic model of the knee was developed to study the interactions between the articulating surfaces of the bones and the geometrical and mechanical properties of the ligaments. The contact-surface geometry of the distal femur, proximal tibia, and patella was modeled by fitting polynomials to each of the eight articular surfaces. Twelve elastic elements were used to describe the function of the ligamentous and capsular structures of the knee. The origin and insertion sites of each model ligament were obtained from cadaveric data reported for an average-size knee. The response of the model to both anterior-posterior drawer and axial rotation suggests that the geometrical and mechanical properties of the model ligaments approximate the behavior of real ligaments in the intact knee. Comparison of the model's response with experimental data obtained from cadaveric knee extension indicate further that the three-dimensional model reproduces the response of the real knee during movement.

Key Words: Knee Model, Knee-Extensor Mechanism, Ligament Model, Dynamics

1. Introduction

The knee is one of the most frequently injured and surgically repaired joints in the body. Almost two million people seek medical care for knee injuries annually.

Most of these injuries are characterized by complex multi-directional displacements that can not be defined or measured objectively. However, surgeon and joint replacement manufacturers can not improve on treatment outcome or longevity of prosthetic tolerance until knee joint injury patterns are accurately defined for the individual patient. The mathematical knee model has been developed to understand the mechanics of the normal knee and for improving the diagnosis of patients with movement disabilities resulting from knee injury. Though numerous attempts have been made to determine the forces transmitted by the human knee, very few models have included the combined interactions of the femur, tibia, and patella (Smidt, 1973; Nisell, 1985; Essinger et al., 1989; Yamaguchi and Zajac, 1989; Garg and Walker, 1990; O'Connor et al., 1990; Tumer and Engin, 1993). It is significant that only two of these studies attempted to model the tibiofemoral and patellofemoral joints in three dimensions (Essinger et al., 1989; Garg and Walker, 1990). In each of these models, however, joint function is not represented completely. In the model developed by Garg and Walker (1990), the relative positions of the femur, tibia, and patella are not calculated. Instead, the displacements of the bones are input to the model using data obtained from cadaveric experiments. Essinger's (1989) model, on the other hand, constrains the movements of the patella to lie along a prescribed path.

In this work, a three-dimensional model of the knee is developed which describes the interactions between the articulating surfaces of the bones and the geometrical and mechanical properties of the ligaments spanning the joint. Quantitative comparisons between model and experiment are also undertaken to assess the rationale of the mechanical and geometrical parameters assumed by the model.

* Technical Center Samsung Motors Inc., Yongin-city Kyungki-Do Korea

2. Articular Surface Geometry of the Knee

An accurate description of the geometry of the articulating surfaces of the bones is critical for accurate calculations of their relative movements. Garg and Walker (1990) measured the geometry of the articular surfaces and ligament attachment sites for 23 normal cadaveric knees. On the basis of these data, we modeled the contact-surface geometry of the femur, tibia, and patella by fitting polynomials to each of the eight articular surfaces (see Fig. 1): the medial and lateral tibial plateaux, the medial and lateral femoral condyles, the medial and lateral patellar surfaces of the femur, and the medial and lateral patellar facets. The coefficients of the polynomials were determined by using optimization theory to minimize errors between the mathematical surfaces and the measured data describing the anatomical shapes of the bones (Foley and van Dam, 1982). Specifically, the medial and lateral femoral condyles were each described by fourth-order polynomials using cylindrical coordinates. A plane approximation was used for both the medial and lateral tibial plateaux. The lateral tibial plateau sloped 7° posteriorly and 2° laterally, while the medial tibial plateau sloped 2° posteriorly and medially. The medial and lateral patellar surfaces of the femoral groove were each represented by second-order polynomials using cylindrical coordinates. The medial and lateral facets of the patella were each also approximated as a flat surface. In the model, the surfaces of the patellar facets were divided by a vertical ridge and inclined at an angle of 130° to one another.

3. Reference Frames

The selection of an appropriate and standardized method for describing three-dimensional joint motion is currently debated by biomechanists interested in providing more direct comparisons between the results obtained from various studies.

In this work, we adopted the coordinate systems given by Kurosawa et al. (1985), Reuben et al. (1989), and Garg and Walker (1990). Kurosawa et al. (1985) showed that the shapes of the posterior femoral condyles may be closely approximated as spheres. The reference frame of the model femur is based on the transverse axis passing through the centers of the near-spherical femoral condyles. The origin of the femoral reference frame is located at the midpoint between the centers of the near-spherical medial and lateral femoral condyles (Kurosawa, et al. 1985) (see Fig. 2). The transverse axis is defined as the x

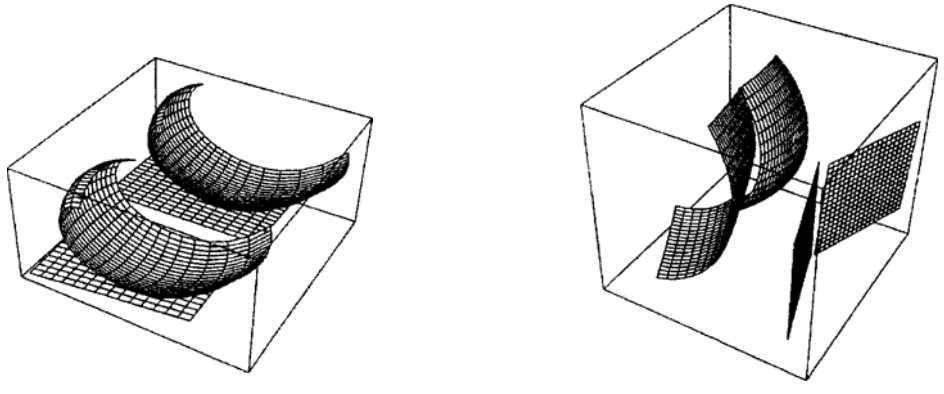

(a) Tibiofemoral joint (b) Patellofemoral joint

Fig. 1 Shapes of the articulating surfaces of the femur, tibia, and patella for the model knee. The tibial plateaux and the surface of each patellar facet were approximated as flat surfaces in the model. The femoral condyles and the surfaces of the femoral groove were modeled by fitting polynomials to the cadaver data reported by Garg and Walker (1990).

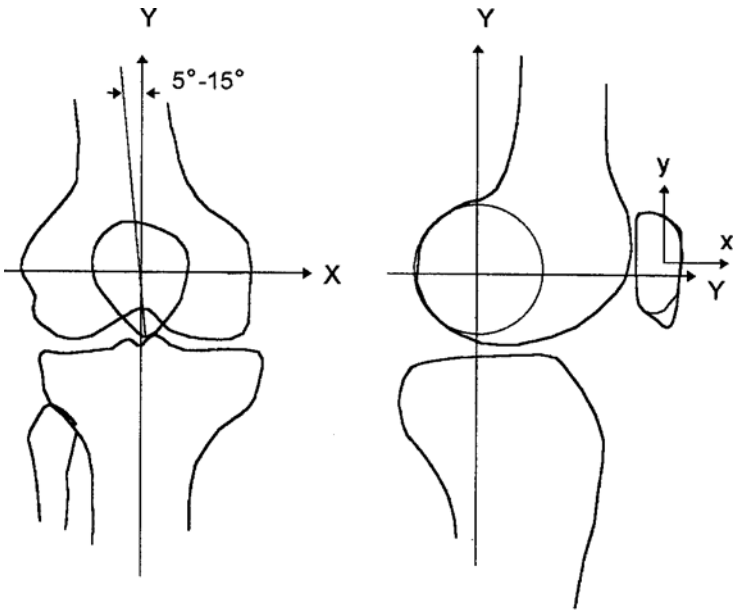

Fig. 2 Reference coordinate frame of the knee: The reference coordinate system of the tibia was defined to be coincident with that of the femur at full extension. The posterior condyles of the femur were shown to closely fit spherical surfaces (Kurosawa et al., 1985). The x-axis was defined as the transverse axis joining the centers of spherical condyles. The y axis was perpendicular to the x-axis and parallel to the long axis of femoral shaft in the sagittal plane. The long axis of the femoral shaft deviated by 5°-15° from y-axis in the frontal plane. The z-axis was determined by vector cross product of x- and y-axes. The origin of the patellar coordinate system was defined as the center of the patella. The axes of the patellar coordinate system were parallel to those of the femoral reference coordinate frame.

-axis of the femur, whose positive direction is taken to point medially. The y-axis is defined to be perpendicular to the transverse axis and parallel to the long axis of the femoral shaft; the y-axis is taken to be positive when pointing toward the hip. The z-axis is formed by taking the vector cross-product of the x and y axes; its direction is positive when pointing anteriorly (see Fig. 2). The femoral reference frame is chosen as the inertial reference frame because this frame remains stationary during flexion-extension movements of the knee.

The origin of the tibial reference frame is defined to be coincident with that of the femoral reference frame when the knee is placed in full extension and no external forces act on the bones. Furthermore, the femoral and tibial reference frames are aligned with one another at full extension. The orientation of the model tibia relative to the model femur is described using Euler angles with the following sequence for three successive rotations of the tibia: x (flexion-extension)-z (varus-valgus rotation)-y (internal-external rotation). The direction of each Euler angle is consistent with the right-hand rule. Note that since the femur remains fixed while the tibia moves, this sequence of joint rotations is identical with that defined by the JCS proposed by the ISB (Wu and Cavanagh, 1995).

In the model, translations of the origin of the tibial reference frame relative to that of the femoral reference frame are expressed in the tibial reference frame. This description of tibial translations is consistent with clinical conventions used by others. Thus, anterior-posterior translations of the tibia relative to the femur are along the z-axis of the tibia; medial-lateral shift is a translation along the x-axis of the tibia; and proximal-distal

distraction is a translation along the y-axis of the tibia.

The origin of the patella reference frame is located at the geometric center of the patella (see Fig. 2). This point was determined from surface measurements (Koh et al., 1992). Thus, at full extension of the knee, the origin of the patellar reference frame is not coincident with the origin of the femoral reference frame. These two reference frames are, however, aligned with each other when the knee is placed in full extension. The orientation of the patella relative to the femur is described by Euler angles with the following sequence for the three successive rotations: x (patellar flexion-extension)-z(patellar rotation) -y(patellar tilt).

Translations of the patella are defined by the position of the origin of the patellar reference frame with respect to the origin of the femoral reference frame. In this case, all translations of the moving body (patella) are expressed in the reference frame of the fixed body (femur).

4. Dynamic Modelling of the Knee

It is assumed that due to synovial fluid, the femoral condyles roll and slide on the tibial plateaux without friction. In the model, the femoral condyles do not necessarily remain in contact with the tibial plateaux at the medial and lateral compartments of the knee. In the real knee, contact between the femur and tibia causes deformation of the bones. In the model, deformation of the bones is calculated by modeling the behavior of cartilage as a thin elastic layer mounted on a rigid foundation which represents the underlying subchondral bone. In contrast to rigid-body contact, where holonomic constraints are derived from imposing geometric compatibility and surface-contact conditions at the joint, the deformable-contact model calculates the contact force by integrating the assumed contact-pressure distribution over the deformed surface area. The resulting forces at the medial and lateral compartments of the knee are then included in the equations of motion in the same way as the concomitant ligamentous and muscle forces. No additional kinematical constraints are necessary when modeling deformable contact in this way. As a consequence, relative movements of the tibia and femur in the model are characterized by six degrees of freedom.

4.1 Model for Deformable Contact at the Tibiofemoral Joint

When the femur and tibia first come into contact with each other, we assume that point contact exists between these bodies. Under the action of the slightest load, the femur and tibia deform in the vicinity of their point of first contact, so that they touch each other over an area which is finite though small compared with the dimensions of the two bodies. We assume further that the contact areas between the femur and tibia remain small in comparison with the dimensions of these bodies, even when muscle forces become relatively large as is the case during maximum, voluntary, isometric contractions. This assumption effectively means that the stresses are highly concentrated in the region close to the contact "patch", and are not greatly influenced by the shape of the bodies at a distance from the contact area. A theory of contact mechanics is needed to predict the shape of this area of contact, and how it might grow in size with increasing tibiofemoral joint load. Furthermore, this theory must allow a calculation of the magnitude and distribution of the surface pressure that is transmitted across the joint. Finally, the theory should enable calculations to be made of the total deformation of each body resulting from the applied load.

4.1.1 Location of the contact point

When the femur and tibia are first brought into contact, a single point of contact is assumed to exist between these two bodies. Note that we do not assume that contact must take place at both the medial and lateral sides of the knee; it is allowable that contact occurs only at one point in the model. At the contact point, a common tangent plane can be found. This common tangent plane ensures that proper contact occurs between the surfaces at the point of contact. To find the location of the contact point, two conditions,

referred to as the *contact conditions,* must be satisfied. First, the tangents and normals to each surface at the contact point must be *parallel:*

$$\boldsymbol{t}_a \bullet \boldsymbol{n}_b = 0 \tag{1}$$

where $\boldsymbol{t}_a$ is the tangent vector to body A (femur) at the contact point, and $\boldsymbol{n}_b$ is the normal vector for body B (tibia) at the contact point. Second, the tangents and normals to each surface at the contact point must be *colinear:*

$$\boldsymbol{t}_a \bullet \boldsymbol{R}_{ab} = 0 \tag{2}$$

where $\boldsymbol{R}_{ab}$ is the vector leading from the contact point on body A (femur) to the contact point on body B (tibia) (see Fig. 3).

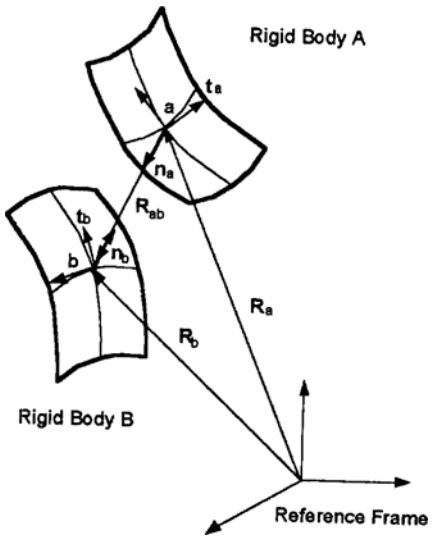

Fig. 3 The contact conditions for the deformable contact model at the tibiofemoral joint. Points a and b represent the points of first contact on bodies A and B, respectively. The vector from point a to point b must be directed along the common normal to both bodies. The condition of hard contact requires coincidence of a and b as an additional constraint. t and n are the tangent and normal vectors for each surface at the points of first contact, point a and point b. $\mathbf{R}_{ab}$ is a position vector which represents the distance between the contact points on the bodies. $\mathbf{R}_a$ and $\mathbf{R}_b$ are vectors which define the position of each contact point relative to a global reference frame.

The location of the contact point was found by solving Eqs. (1) and (2) simultaneously using a root-finding algorithm for nonlinear equations. Note that only the two contact conditions are used to find the location of the contact point for the tibiofemoral joint model. If the bodies were rigid, an additional constraint equation is needed to prevent interpenetration of the two surfaces (see Sec. 4. 2). Because our model for the tibiofemoral joint assumes that the surfaces deform under load, this kind of condition is not imposed.

4.1.1 Shape of the contact area

Begin by letting the point of first contact be the origin of a rectangular coordinate system in which the x-y plane is the common tangent plane to the two surfaces, and the z-axis lies along the common normal directed positively into the lower solid (see Fig. 4(a)). The geometry of the femur and tibia in the region of the point of first contact is approximated; the shape of each surface in the vicinity of the contact region is described by a second-order surface polynomial (Johnson, 1985). When each of these surfaces is projected onto the tangent plane at the point of contact, the projected shape is an ellipse (Johnson, 1985). Based upon the theory of Hertz, when the two bodies are then brought into contact and loaded, the shape of the resulting contact area is also an ellipse.

By choosing the orientation of the x and y axes so that the term in xy vanishes, the separation between the surfaces, z, may be written as

$$z = Ax^2 + By^2 = \frac{1}{2\rho_e}x^2 + \frac{1}{2\rho_e'}y^2 \tag{3}$$

where A and B are positive constants, as yet unknown, and ρ_e and ρ_e' are the principal relative radii of curvature whose values are also unknown. Physically, ρ_e and ρ_e' represent the principal radii of curvature of the ellipse that results when the individual ellipses for bodies A and B are added together. The problem, therefore, is to calculate values for the constants A and B, from which the principal relative radii of curvature, ρ_e and ρ_e', may then be found.

Johnson (1985) has shown that if the axes of principal curvature of each surface, the x_a axis and the x_b axis say, are inclined to each other at an angle of Ψ (see Fig. 4(b)), then the constants A and B may be found by solving the following two equations simultaneously:

$$B+A=\frac{1}{2}\left[\frac{1}{\rho_a}+\frac{1}{\rho'_a}+\frac{1}{\rho_b}+\frac{1}{\rho'_b}\right] \tag{4}$$

$$B-A=\frac{1}{2}\left[\left(\frac{1}{\rho_a}-\frac{1}{\rho'_a}\right)^2+\left(\frac{1}{\rho_b}-\frac{1}{\rho'_b}\right)^2+2\left(\frac{1}{\rho_a}-\frac{1}{\rho'_a}\right)\left(\frac{1}{\rho_b}-\frac{1}{\rho'_b}\right)\cos 2\Psi\right]^{1/2} \tag{5}$$

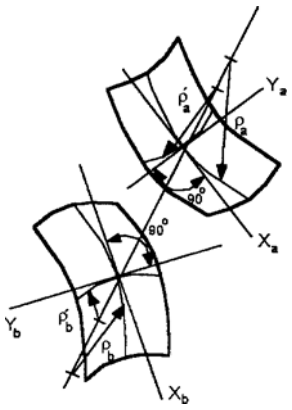

(a) Two Solid elast bodies

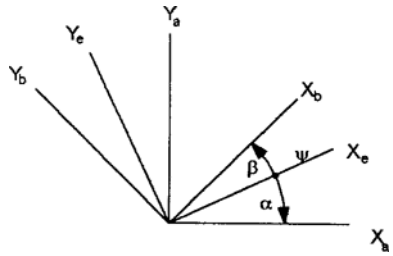

(b) First-quadrant projection of principal curves

Fig. 4 Principal radii of curvatures at the contact point. The two bodies are pressed together so that the z-axis is the common normal. ρ and ρ' represent the principal radii of each surface. X and Y represent projections of the planes containing the principal radii on the tangential plane at the point of contact. The principal planes of the two contacting surfaces are inclined to each other at an angle Ψ. X_e and Y_e are the projections of the penetrated surface after contact. α and β are the angles between the planes of the principal radii of the contacting surfaces and those of the penetrated surface.

where ρ_a, ρ'_a, ρ_b, and ρ'_b are the principal radii of curvatures for the contacting surfaces, and Ψ is the angle between the axes which coincide with the principal radii of curvatures, ρ_a and ρ_b (see Fig. 4(b)).

Once Eqs. (4) and (5) have been solved simultaneously for the constants A and B, the principal relative radii of curvature of the elliptical contact area, ρ_e and ρ'_e, may be found from

$$\rho_e=\frac{1}{2A} \tag{6}$$

$$\rho'_e\frac{1}{2B} \tag{7}$$

Finally, if x_e denotes the axis which coincides with the principal radius of curvature ρ_e, then the angles between x_e, x_a, and x_b are given by (see Fig. 4(b)):

$$\tan\beta=\frac{\left(\frac{1}{\rho_a}-\frac{1}{\rho'_a}\right)\sin 2\Psi}{\left(\frac{1}{\rho_b}-\frac{1}{\rho'_b}\right)-\left(\frac{1}{\rho_a}-\frac{1}{\rho'_a}\right)\cos 2\Psi} \tag{8}$$

$$\alpha=\Psi-\beta \tag{9}$$

where α is the angle between the axes coinciding with the principal radii ρ_e and ρ_a, and β is the angle between the axes coinciding with the principal radii ρ_e and ρ_b (Fig. 4(b)).

4.1.3 Calculation of the resultant contact force

The elastic-foundation model is used to calculate the pressure distributions and resultant contact forces at the medial and lateral compartments of the tibiofemoral joint. This model combines the layers of cartilage on the posterior femoral condyles and on the tibial plateaux into a single, elastic layer of depth h. Furthermore, the model assumes that the elastic layer rests on a rigid foundation of subchondral bone. The elastic-foundation approach has been used by others to calculate the forces transmitted at the knee (Andriacchi et al., 1983; Essinger et al., 1989; Blankevoort et al., 1991).

If the penetration at the origin is denoted by δ,

then the total normal elastic displacements of the cartilage layer are given by

$$u_{z_a}+u_{z_b}+z=\delta \tag{10}$$

where u_{z_a} and u_{z_b} represent the normal elastic displacements of the cartilage layer on bodies A and B, respectively. Thus, $u_{z_a}+u_{z_b}$ represents the combined normal elastic displacement of the cartilage layer foundation. Substituting Eq. (3) into Eq. (10) gives an expression for the total normal elastic displacement of the cartilage layer at any point (x, y) within the contact area, thus:

$$u_z(x,\ y)=\delta-\left(\frac{x^2}{2\rho_e}\right)-\left(\frac{y^2}{2\rho_e'}\right) \tag{11}$$

The penetration at the origin of the coordinate system, δ, is the maximum normal displacement of the cartilage layer, and is given by (see Fig. 5)

$$\delta=(\boldsymbol{R}_a-\boldsymbol{R}_b)\bullet\boldsymbol{n} \tag{12}$$

where $\boldsymbol{R}_a$ and $\boldsymbol{R}_b$ are, respectively, the position vectors of the contact points on body A and body B, relative to the origin of the femoral reference frame (see Fig. 4), and $\boldsymbol{n}$ is the unit vector directed along the common normal of the contacting surfaces at the contact point.

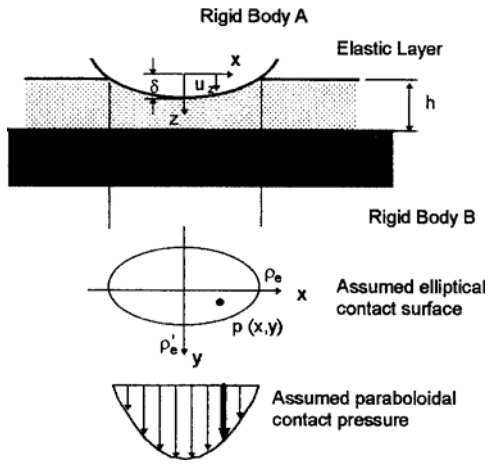

Fig. 5 Elastic-foundation model used to calculate the pressure distributions and resultant forces acting at the medial and lateral sides of the tibiofemoral joint. The z-axis is the common normal at the point of contact. The contact pressure at any point within the contact area depends on the displacement u_z The profile of the pressure distribution is assumed to be paraboloidal rather than ellipsoidal as given by the Hertzian theory of contact between two elastic bodies. The transverse section of the deformed elastic layer is assumed to be an ellipse.

Assuming that the pressure at any point (x, y) depends only on the displacement at that point (i. e., shear between the adjacent elements of the layer is neglected), and that it increases with increasing normal displacement of the cartilage layer, the contact pressure (p) at any point within the contact area can be written as (Blankevoort et al., 1991):

$$dp=K\frac{d\left(\frac{u_z}{h}\right)}{1-\frac{u_z}{h}} \tag{13}$$

where K is the *equivalent or bulk* modulus of cartilage, and h is the total thickness of the foundation layer.

Under the assumption of uniaxial, confined compression (i. e., no lateral expansion of the layer occurs so that the radial and tangential strains remain zero), it can be shown that Hooke' s law leads to the following expression for the bulk modulus of the layer, K (Dowson and Taylor, 1967; Dowson and Jin, 1990; Blankevoort et al., 1991):

$$K=\frac{(1-\nu)}{(1+\nu)(1-2\nu)} \tag{14}$$

where E and ν are the Young's modulus and Poisson's ratio of cartilage, respectively. Equation (14) is valid only when the normal displacements of the cartilage layer within the contact area remain *small.*

We modeled cartilage as a single-phase, linear, elastic material, and assumed that its properties are both homogeneous and isotropic. Approximating cartilage as a single-phase, elastic material is not justifiable if its long-term response is to be modeled. This is because the long-term response of this tissue exhibits the nonlinear, viscoelastic properties of creep and stress relaxation. When cartilage is loaded over a short period of time, however, say in the range of 1-5 seconds, its response is more-or-less elastic (Hayes and Bodine, 1978; Hori and Mockros. 1976; Mak,

1986). In the cadaveric knee experiments performed in the previous work, quadriceps forces were applied for no longer than 5 seconds (Kim, 1998). Therefore, we took the value of the elastic modulus of cartilage to be E=5 MPa, and the value of Poisson's ratio as $\nu=0.45$. These values are similar to those assumed by Blankevoort et al. (1991).

Finally, the resultant force transmitted at the joint is found by integrating the pressure distribution acting within the contact area. For the nonlinear model of cartilage, the resultant contact force is given by

$$P=-K\frac{\pi ab}{\frac{\delta}{h}}\left[\frac{\delta}{h}+\ln\left(1-\frac{\delta}{h}\right)\right] \tag{15}$$

where a and b are parameters of the ellipse given by

$$a=(2\delta\rho_e)^{1/2},\ b=(2\delta\rho_e')^{1/2} \tag{16}$$

Note that, in each case, the resultant force is assumed to act at the centroid of the elliptical contact area.

4.2 Model of the Patellofemoral Joint

The knee-extensor mechanism, which describes the interaction between the quadriceps tendon, patellar ligament, and patella, acts to improve the leverage of the quadriceps muscles at the knee. Several mathematical models of the patellofemoral joint have appeared in the literature (van Eijden et al., 1986; Yamaguchi and Zajac, 1989; Hirokawa, 1991; Hefzy and Yang, 1993; Heegard et al., 1995). The model developed in this study is, in many respects, similar to that described by Hirokawa (1991).

We assumed that the patella could be approximated as a massless body. This assumption is reasonable since the mass of the patella is negligible in comparison with the mass of either the thigh or the shank. The surfaces of the patellar facet and femoral groove were also assumed to be frictionless. Under these assumptions, only four forces act to equilibrate the patella at any given angle of the knee: the force applied by the quadriceps tendon, the force developed in the patellar ligament, and the two contact forces acting at the medial and lateral sides of the patellofemoral joint. Note that the force applied to the model patella by the quadriceps tendon is the resultant force developed by the four separate heads of the quadriceps muscles included in the model: rectus femoris (RF), vastus medialis (VMED), vastus intermedius (VINT), and vastus lateralis (VLAT)).

Three holonomic constraints act to restrict the motion of the patella relative to the femur and tibia in the model. By assuming rigid-body contact in our model for patellofemoral mechanics, *point contact* exists between the femoral groove and patellar facet at both the medial and lateral sides of the knee. Equations (1) and (2) are used to calculate the location of the contact point at each side of the patellofemoral joint. These parameters are then used in the equation for geometric compatibility to obtain the required holonomic constraint. The geometric compatibility condition ensures that no interpenetration takes place between the surfaces of the femur and patella at each contact point. Thus,

$$\boldsymbol{R}_{ab}\bullet\boldsymbol{n}=\boldsymbol{0} \tag{17}$$

where $\boldsymbol{n}$ is the common normal at the contact point for body A (patella) and body B (femur). In addition, the patellar ligament was assumed to be inextensible, in which case one point on the patella was constrained to lie on a sphere whose radius was equal to the length of the patellar ligament in the model. Motion of the patella, when in contact with the femur, was therefore characterized by *three* degrees of freedom.

This simplification in the model is not as limiting as it might first appear to be. In the natural knee, cartilage deforms at both the tibiofemoral and patellofemoral joints as the bones are pressed together by the action of the muscles. One of our major interests in developing a mathematical model of the knee is to use the model to calculate cruciate and collateral ligament forces during activity. Knee-ligament forces are affected by the degree to which cartilage and the menisci are compressed under tibiofemoral load. It is assumed, however, that deformation of cartilage on the patellar facet and on the medial and lateral

patellar surfaces of the femoral condyles will have much less of an effect on the forces developed by the cruciate and collateral ligaments of the knee. For this reason, the mechanical behavior of cartilage was neglected in our model of the patellofemoral joint.

4.3 Model of the Ligaments

Twelve separate bundles were used to model the geometrical and mechanical behavior of the cruciate ligaments, the collateral ligaments, and the posterior capsule of the knee (see Fig. 6(a) and (b)). The anterior cruciate ligament (ACL) and the posterior cruciate ligament (PCL) were each modeled by two fiber bundles, one to represent the most anterior, and the other to represent the most posterior portion of the ligament (Girgis et al. 1975). The lateral collateral ligament (LCL) was modeled using only one bundle. The medial collateral ligament (MCL) was separated into two layers: a superficial layer represented by three bundles, and a deep layer represented by two other bundles. The actions of the posterior capsule, arcuate ligament, and oblique popliteal ligament were combined and represented by a medial and a lateral bundle.

The origin and insertion sites of all the ligaments, except the deep bundles of the MCL and the posterior capsule, were obtained from Garg and Walker (1990). Attachment sites of the deep MCL and the posterior capsule were based on data reported by Blankevoort et al. (1991) and by Reicher (1993). The path of each model ligament bundle was approximated by a straight line running from its origin on the femur to its insertion on the tibia. Contact of the ligaments with bone and with the other ligaments of the knee was not taken into account in the model.

Each ligament bundle was assumed to be elastic, and its mechanical behavior was represented

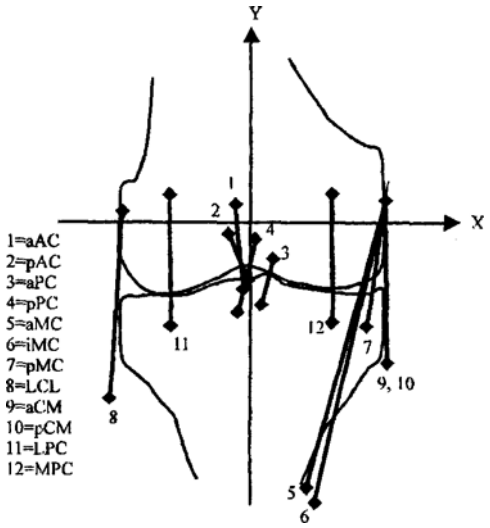

(a) The geometry of the model ligaments in the frontal plane

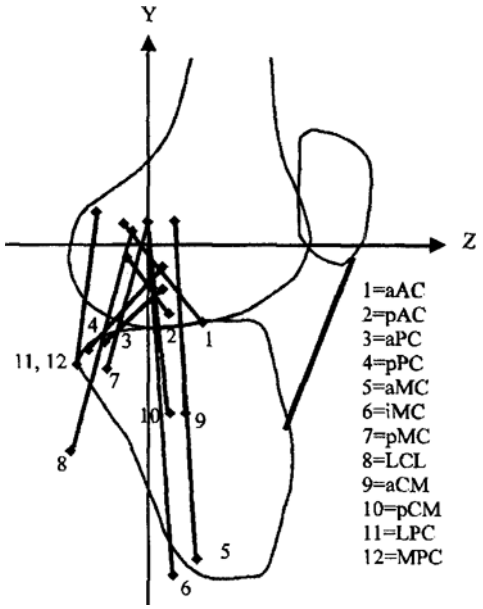

(b) The geometry of the model ligaments in the sagittal plane

Fig. 6 Schematic of the model knee showing the location of the model ligament bundles. Twelve ligament bundles were included in the model. Symbols appearing in the diagram are: a AC, anteromedial bundle of the ACL; pAC, posterolateral bundle of the ACL; aPC, anteromedial bundle of the PCL; pPC, posterolateral bundle of the PCL; aMC, anterior bundle of the superficial fibers of the MCL; iMC, intermediate bundle of the superficial fibers of the MCL; pMC, posterior bundle of the superficial fibers of the MCL; aCM, anterior bundle of the deep fibers of the MCL; pCM, posterior bundle of the deep fibers of the MCL; LCL, lateral collateral ligament; LPC, lateral posterior capsule; MPC, medial posterior capsule.

by a nonlinear stress-strain curve (Butler et al., 1986). Specifically, the force in each model ligament bundle was assumed to be quadratic for low strains, and linear for strains beyond a prespecified point corresponding to twice the linear strain limit:

$$\begin{aligned} f&=\frac{k\varepsilon^2}{4\varepsilon_l} \quad 0\le\varepsilon\le 2\varepsilon_l \\ f&=k(\varepsilon-\varepsilon_l) \quad \varepsilon>2\varepsilon_l \\ f&=0 \quad \varepsilon<0 \end{aligned} \tag{18}$$

Here, f is the tensile force in the model ligament bundle, k is its stiffness (i. e., force per unit strain), and ε is the strain in the model ligament bundle, defined as the ratio of its instantaneous increase, $L-L_o$, to the assumed value of its reference length, L_o. The linear strain limit ε_l was set to 0.03 for all the ligaments in the model (Butler et al., 1986). The viscoelastic properties of the ligaments, such as creep and force relaxation, were neglected in the model.

The ligament reference length, L_o, can be calculated from values of the reference strains in full extension. Unfortunately, no experimental data are available for the reference strains of knee ligaments. These parameters, together with the values of ligament stiffness, were determined by matching the overall stiffness and laxity of the model knee with experimental data reported in the literature (see below). Table 1 gives the values of stiffness and reference strain assumed for each ligament bundle in the model.

Table 1 Values of stiffness and reference strains assumed for the model ligaments.

Ligament	Ligament Budle	Stiffness: force/strain (N)	Referenct strain (ε_r)
Anterior cruciate (ACL)	aAC	1500	0.02
	pAC	1600	0.02
Posterior cruciate (PCL)	aPC	2600	−0.21
	pPC	1900	0.02
Medial collateral (MCL)	aMC	2500	0.05
	iMC	3000	0.04
	pMC	2500	0.02
	aCM	2000	−0.08
	pCM	4500	0.03
Lateral collateral (LCL)	LCL	2000	0.02
Posterior capsule (pCap)	LPC	1500	0.06
	MPC	1500	0.06

4.4 Quadriceps leg raise simulation of the model

The aim of the quadriceps leg raise simulation is to assess the accuracy of the model calculations by comparing the response of the model knee with measurements obtained from the cadaveric experiments described in Kim (1998). In these experiments, the intact knee was extended by a known force applied to the quadriceps tendon, with and without weights attached to the ankle. All soft tissues surrounding the knee, except the capsular structures and quadriceps tendon, were removed by dissection. The rate at which the knee was extended was controlled by specifying the rate of change of length of the cable connecting the quadriceps tendon to a stepper-motor (see Fig. 7). To emulate the conditions of the experiment, all muscles, except rectus femoris, were removed from the model. The force developed by this muscle in the model was assumed to be independent of its length, velocity, and activation level, so that it may approximate the action of the wire cable used in the experiments. In the model, as in the experiments, the rate of knee extension was controlled by specifying a trajectory for the rate of change of the quadriceps muscle length in time. Specifically, the model simulated a quadriceps leg raise which took about 20 seconds to extend the knee from 90° of flexion to full extension.

The dynamical equations governing motion for the quadriceps leg raise simulation can be written as (see Fig. 8):

$$\begin{aligned} &A(\boldsymbol{q}_{tf})\,\ddot{\boldsymbol{q}}_{tf}+B(\boldsymbol{q}_{tf},\,\dot{\boldsymbol{q}}_{tf})\,\boldsymbol{q}_{tf}+G(\boldsymbol{q}_{tf}) \\ &+M_{1ig}(\boldsymbol{q}_{tf})\,F_{1ig} \\ &+M_{tf}(\boldsymbol{q}_{tf})\,F_{tf}+M_{p1}(\boldsymbol{q}_{tf})\,F_{p1}+\boldsymbol{J}^T F_q=0 \end{aligned} \tag{19}$$

$$L_q=f(t);\ \text{quadriceps muscle length} \tag{20}$$

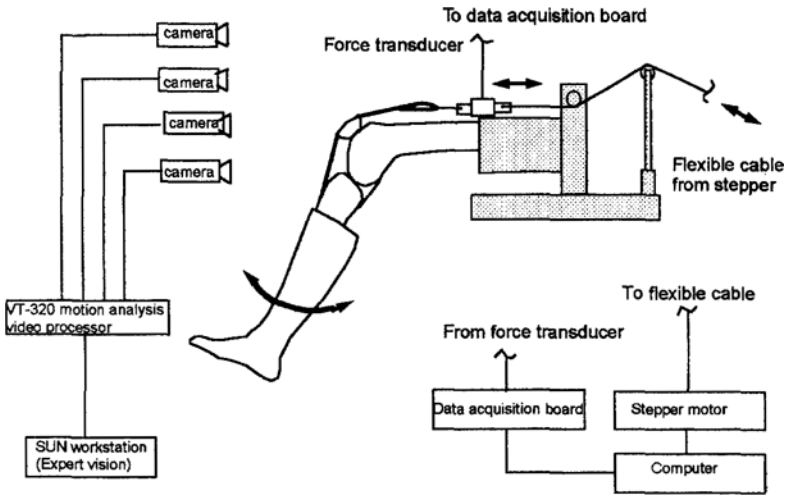

Fig. 7 Schematic drawing of the experimental test rig for the quadriceps leg raise task. The femur was mounted horizontally and fixed to the frame of the table, while the tibia hung vertically by its weight. The flexible wire cable was attached to the quadriceps tendon. The stepper motor controlled the length of the flexible wire causing the knee to extend at a prescribed rate. The force in the wire cable (quadriceps force) was measured during flexion-extension movements of the knee. The motion analysis system measured the relative displacements of the femur, tibia, and patella during the leg raise task (adapted from Kim, 1998).

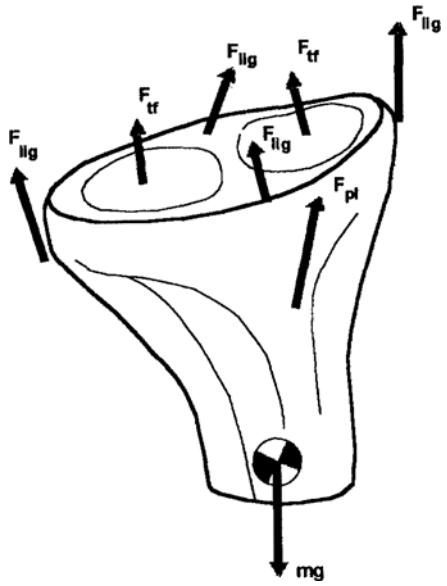

Fig. 8 Free-body diagram of the tibia. F_{tf} are the forces acting at the medial and lateral sides of the tibiofemoral joint; F_{lig} are the forces due to the ligamentous and capsular structures of the knee; F_{pt} is the force in the patellar ligament; mg is the weight of the tibia.

where $\boldsymbol{q}_{tf}$, $\dot{\boldsymbol{q}}_{tf}$, and $\ddot{\boldsymbol{q}}_{tf}$ are 6×1 vectors specifying the displacements, velocities, and accelerations of the tibia relative to the femur; $M_{lig}(\boldsymbol{q}_{tf})$ is a $6\times n$ matrix which contains the moment arms of the model ligament bundles, each calculated about the origin of the tibial reference frame; n is the number of ligament bundles included in the model ($n=12$; see Sec. 4. 3); $M_{pt}(q_{tf})$ is a 6×2 matrix containing the moment arms of the contact forces acting at the medial and lateral sides of the tibiofemoral joint, each calculated about the origin of the tibial reference frame; $M_{pt}(\boldsymbol{q}_{tf})$ is a 6×1 matrix containing the moment arm of the patellar ligament force calculated about the origin of the tibial reference frame; F_{tf} are the tibiofemoral forces which act normal to the contacting surfaces on the medial and lateral sides of the joint; Flig are the ligament forces acting on the tibia; $A(\boldsymbol{q}_{tf})$ is the 6×6 system mass matrix; $G(\boldsymbol{q}_{tf})$ is a 6×1 vector containing only gravitational terms; and $B(\boldsymbol{q}_{tf}, \dot{\boldsymbol{q}}_{tf})$ is a 6×1 vector describing both Coriolis and centrifugal effects; $J(q)$ is a 6×1 matrix, called the constraint Jacobian of the kinematical constraint given by Eq. (20). Specifically, $J^T F_q$ represents the con-

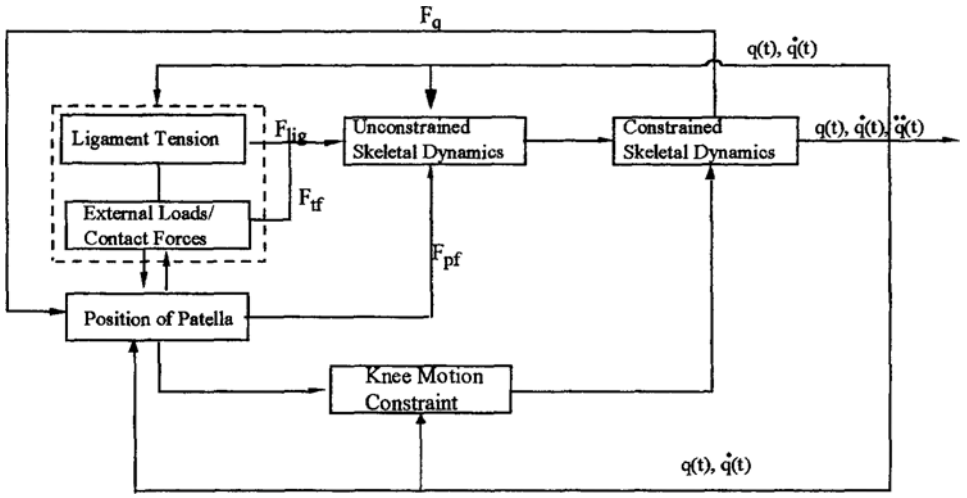

Fig. 9 Block diagram showing interactions among the major compartments of the ligamentous skeletal model with knee motion constraints.

straint forces and torques that must be applied to the model tibia in order to control the length of the quadriceps muscle.

Equations (19) and (20) were generated symbolically using a commercial software package called SD/Fast (Symbolic Dynamics Inc.). They represent a set of 6 nonlinear, *differential* equations which must be numerically integrated using a variable-step, Runge-Kutta-Feldberg 5-6 integrator, given an appropriate set of initial conditions and applied forces. Because integrating equations of motion for constrained dynamical systems usually introduces error during the integration procedure, we used Baumgarte's method within SD/Fast to stabilize and reduce the integration errors. Figure 9 shows the interactions between the major components of the model for the quadriceps leg raise simulation.

5. Stiffness and Laxity of the Model Knee

In this section, we assess the rationale of the ligament properties assumed by the model, specifically the origin and insertion sites and the values of stiffness and reference strain for each ligament bundle in the model. Although the stiffnesses and origin and insertion sites of the cruciate and collateral ligaments of the knee are available in the literature, values of ligament reference strains cannot be obtained from measurements performed on cadaveric knees. Our approach for assessing the rationale of the model ligament parameters is to compare the anterior-posterior stiffness and torsional stiffness of the model knee with data obtained from cadaveric experiments reported in the literature (e. g., Markolf et al., 1976).

5.1 Anterior-posterior stiffness

The response of the model to anterior-posterior drawer compares favorably with experimental data reported by Markolf et al. (1976, 1981), Butler et al. (1980), Piziali et al. (1980) and Fukubayashi et al. (1982) for knee flexion angles of 0°, 20°, 30°, and 90° (Fig. 10). The response of the model was compared with the experimental data at these particular angles of flexion because the real knee is known to be much stiffer at the extreme angles of flexion (i. e., full extension and 90° of flexion) than at either 20° or 30° of flexion. In fact, it is for this reason that the Lachman Test is used rather than the Drawer Test when the joint is tested for partial or complete rupture of the ACL.

Consistent with the experiments, the stiffness of the model knee is lower at moderate values of flexion (20° and 30° of flexion) than at the extremes (full extension and 90° of flexion) (Fig.

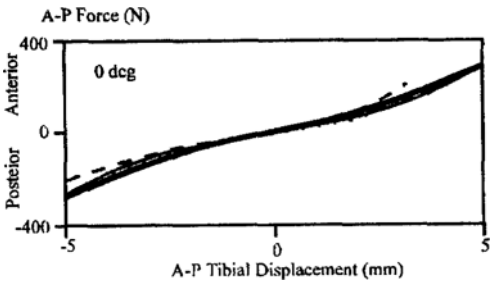

(a) Knee flexion 0° : Markolf et al. (1981) (dotted line), Piziali et al. (1980) (light solid line), Shoemaker et al. (1985) (dashed line)

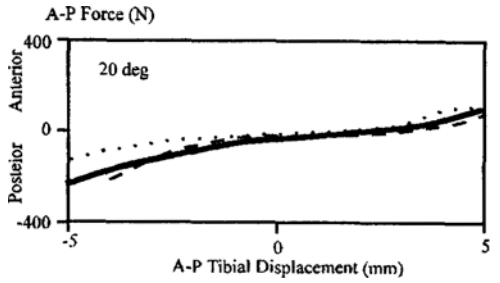

(b) Knee flexion 20° : Markolf et al. (1991) (dotted line), Shoemaker et al. (1985) (dashed line)

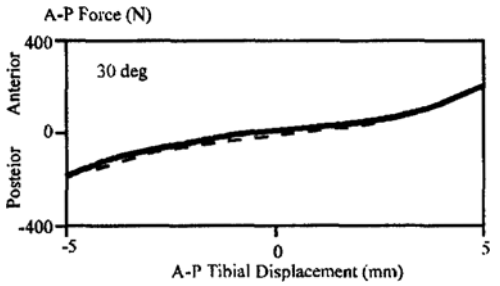

(c) Knee flexion 30° : Fukubayashi et al. (1982) (dashed line)

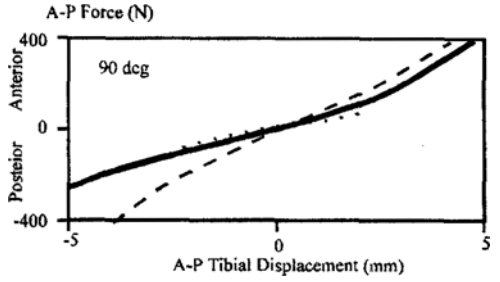

(d) Knee flexion 90° : Butler et al. (1980) (dashed line), Markolf et al. (1976) (dotted line)

Fig. 10 Anterior-posterior force-displacement curves at 0, 20, 30, and 90° of knee flexion. Anterior-posterior force for the model (heavy solid line) was calculated for values of anterior-posterior drawer ranging from -5 to 5 mm. At each knee angle, a neutral value of anterior-posterior translation of the tibia relative to the femur was first found. This was the tibiofemoral translation at which all of the ligament forces were completely balanced. The tibia was then translated a given amount either anteriorly (positive translation) or posteriorly (negative translation) and the corresponding A-P force calculated. In the model, and as assumed in the experimental studies, this A-P force was due entirely to the ligaments and capsular structures.

10, compare heavy solid line with light solid, dashed, and dotted lines). This is because at 20° and 30° of flexion, there is a small region around the neutral position at which all of the ligament forces remain small (Fig. 10(b) and (c)). That is, the knee is relatively lax at these angles of flexion. At small and large angles of flexion, however, both the model and the experiments show that the ACL and PCL bear load for nearly all values of drawer (Fig. 10(a) and (d)). Thus, the knee becomes relatively *stiff* at the extreme angles of flexion.

5.2 Internal-external (torsional) stiffness

The model and the experiments show that the knee is most stable at full extension since torsional laxity is minimum in this configuration, whereas at more flexed positions it is less stable because torsional laxity increases substantially (Markolf et al. 1976 and Blankevoort et al. 1988). In the real knee, torsional laxity increases rapidly from full extension to about 20° or 30° of flexion, after which it remains relatively constant (Fig. 11, compare dotted lines at 0°, 20°, 30°, and 90° of flexion). This behavior is generally reproduced by the model, although torsional laxity in the model continues to increase as knee flexion angle increases, whereas laxity in the real knee remains relatively constant at all angles greater than about 45° of flexion (Fig. 11, compare heavy solid line with light solid and dotted lines from 45° to 90° of flexion). Furthermore, for both internal and

external rotation, torsional laxity is noticeably greater in the model than in the real knee at large angles of flexion. The unstable torsional laxity at large angles of knee flexion can be explained by the effects of ligaments which are not included the model (Kim, 1996). The only structure preventing translation and rotation of the tibia on the lateral side of the model knee is the LCL. Absent from the model, therefore, are the anterolateral structures, consisting of the iliotibial band and midlateral capsule, and the posterolateral structures consisting of the popliteus tendon and the posterolateral capsule. Each of these structures, together with the LCL, ACL, and PCL, provides substantial restraint to external and internal rotation of the tibia.

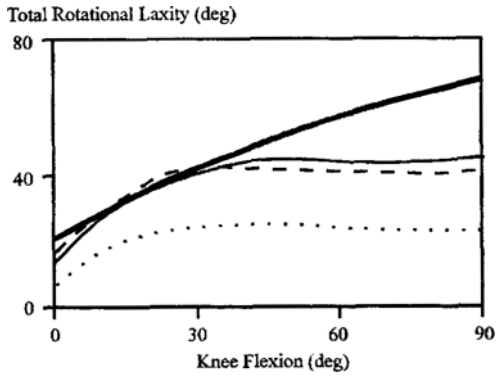

Fig. 11 Total rotational laxity calculated for the model (heavy solid line) for applied torques of ± 3 Nm plotted against knee flexion. At each knee angle, a neutral value of anterior-posterior translation of the tibia relative to the femur was first found. This was the tibiofemoral translation at which all of the ligament forces were completely balanced. Torques of ± 3 Nm were then applied to the tibia either internally (positive rotation) or externally (negative rotation) and the corresponding rotation calculated. The total laxity of the model is the total amount of tibial rotation between the limits of internal-external rotation. Experimental data (light solid, dotted, dashed lines) were obtained from the following studies: Markolf et al. (1976) (dotted line), Blankevoort et al. (1988) (light solid line), Nielsen et al. (1984) (dashed line).

6. Comparison of Model and Experiment for uadriceps Leg Raise

Quantitative comparisons between the response of the model and experimental data can be used to verify the accuracy of the model calculations. More often than not, however, they reveal the deficiencies of the model. In this section, the response of the model is compared with data obtained from the quadriceps leg raise experiments described in Kim (1998). Model calculations for the applied quadriceps force and for the associated displacements of the tibia and patella relative to the femur are quantitatively compared against measurements obtained from three intact, cadaveric knees.

6.1 Applied quadriceps force

When comparing model and experiment, it is critical that the loading conditions and constraints be the same in both. To show this, we have plotted the quadriceps force required to extend the lower leg in the model and in the experiments for each of the three specimen knees (Fig. 12). Consistent with the experiments, quadriceps force in the model remains relatively constant in the range 20 °-60 ° of knee flexion. As noted in Kim (1998), this results from the fact that the ratio of moment arms of the patellar ligament force and leg weight, each calculated about the tibiofemoral contact point, varies little in this region. As the knee approaches 90 ° of flexion, quadriceps force decreases to zero as the cosine of the knee angle approaches zero.

At all angles of flexion, except near full extension of the knee, quadriceps force in the model, normalized to body weight, is in close agreement with that measured for two of the specimens tested (Figs. 12, compare heavy solid line with dashed and dotted lines). Interestingly, these results differ quite noticeably from that obtained for the third specimen tested (Figs. 12, compare heavy solid and light solid lines). Differences between the applied quadriceps force for the specimens tested in this study are presumably due to anatomical differences between the specimens.

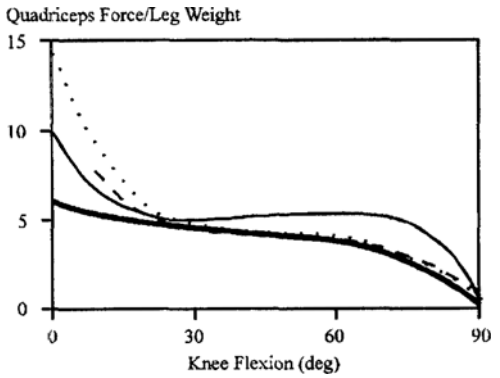

Fig. 12 Comparison of quadriceps force needed to extend the model knee (heavy solid line) and the intact cadaveric knees during the leg raise task. In the model, and in the cadavers, the lower leg comprised the shank and the foot. Experimental data are shown for the three specimens tested in this study: specimen 1 (solid line), specimen 2 (dashed line), and specimen 3 (dotted line). Quadriceps force in the model is generally lower than that needed to extend the cadaveric knees, particularly near full extension.

The most significant difference between the quadriceps force calculated in the model and that applied to the cadavers occurs near full extension of the knee. For each of the specimens tested, the quadriceps force required to extend the knee increases rapidly near full extension (light solid, dashed, and dotted lines in Figs. 12). For the model, however, relatively little additional force is needed in the quadriceps to bring the knee to full extension. There are two likely explanations for this result. First, our model may not accurately reproduce the behavior of the posterior capsule, which begins to tighten near full extension of the knee (O'Connor et al., 1990). Second, our model does not account for contact of the ACL with the roof of the intercondylar notch (Norwood and Cross, 1977). This effect presumably causes the ACL to tighten near full extension, thereby requiring higher quadriceps forces to extend the knee in this region of flexion.

6.2 Relative displacements of the knee

There is a limited level of agreement between the response of the model and the cadaveric measurements of tibial displacements for the leg raise task (Fig. 14, compare heavy solid line with light solid, dashed, and dotted lines). The model and the cadavers exhibit internal rotation and anterior translation of the tibia relative to the femur as the knee is flexed from full extension to 90° (Fig. 13(a) and (e)). Consistent with the motion of the real knees, the model tibia rotates *internally* by as much as 20° when the knee is brought to full flexion (Fig. 13(a), heavy solid line). Most of this rotation, however, is confined to the final 30° of knee flexion. In contrast, a large portion of internal tibial rotation measured in at least two of the specimens occurs during the first 30° of knee flexion (light solid, dashed, and dotted lines in Fig. 13(a)).

The above represents an important difference between the model and the experiments for it suggests that the model is not able to reproduce the screw-home mechanism during the final 30° of knee extension. Notice, however, that one of the specimens tested in this study also does not display the characteristic screw-home mechanism (Fig. 13(a), compare dotted lines from 0°-30° of flexion). Differences between model and experiment in this respect, and for that matter between the specimens themselves, may be due either to differences in the geometry of the bones or to differences in the line of action of the patellar ligament force relative to the long axis of the tibia.

In general, and consistent with the experimental measurements, the model tibia translates *anteriorly* as the knee flexes from full extension to 90° (Fig. 13(e), compare heavy solid line with light solid, dashed, and dotted lines). Peak anterior translation of the tibial origin in the model is around 7 mm, which is close to that measured in two of the specimen knees. Notice, however, that the model tibia also translates a small amount posteriorly as the knee flexes from 30° to 60° (Fig. 13(e), heavy solid line). Only one of the cadavers exhibited this behavior near full extension of the knee.

The model calculations show that the tibia tilts first medially (varus rotations) and then laterally

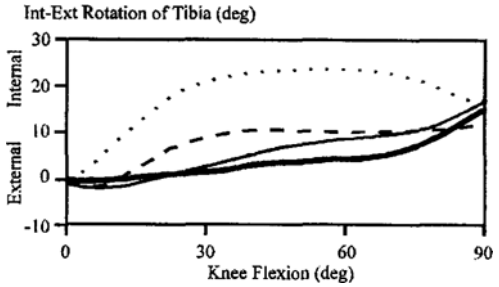

(a) Internal-external rotation of the tibia: internal rotation (positive); external rotation (negative)

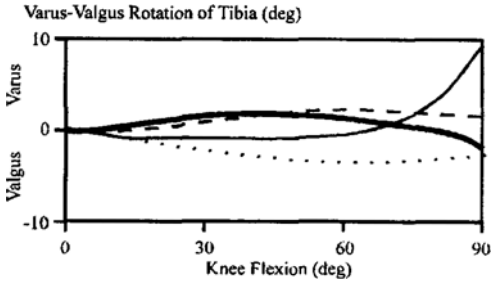

(b) Varus-valgus rotation of the tibia: varus of the tibia (positive); valgus of the tibia (negative)

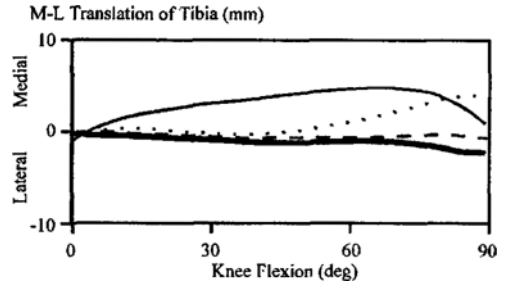

(c) Medial-lateral translations of the tibia: medial translation (positive); lateral translation (negative)

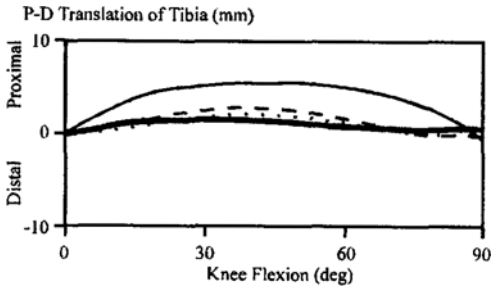

(d) proximal-distal translations of the tibia: distal translation (positive); proximal translation (negative)

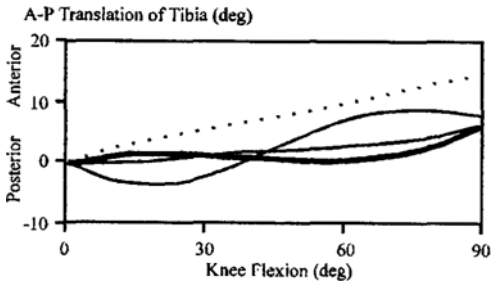

(e) Anterior-posterior translations of the tibia: anterior translation (positive); posterior translation (negative)

Fig. 13 Comparison of the movements of the tibia relative to the femur in the model (heavy solid lines), and in the intact cadaveric knees, for the quadriceps leg raise. The displacements of the tibia in the model and in the cadavers were measured relative to the position and orientation of the bone when the knee was placed in full extension (i.e., the reference configuration of the leg). Shown are the measured rotations and translations of the tibia relative to the femur for the three specimens tested in Kim (1997): specimen 1 (solid line), specimen 2 (dashed line), and specimen 3 (dotted line).

(valgus rotations) during flexion of the knee (Fig. 13(b), heavy solid line). Although the measurements of varus-valgus rotations of the tibia in the cadavers are variable, these angles generally lie below 5°. The behavior of the model is consistent with the measurements in this respect.

The measurements also show that the tibial origin translates medially and *proximally* for the entire range of knee flexion (dotted lines in Fig. 13(c) and (d)) In contrast, the model tibia translates proximally and *laterally* as the knee flexes to 90° (Figs. 13(c) and (d), compare heavy solid line with light solid, dashed, and dotted lines).

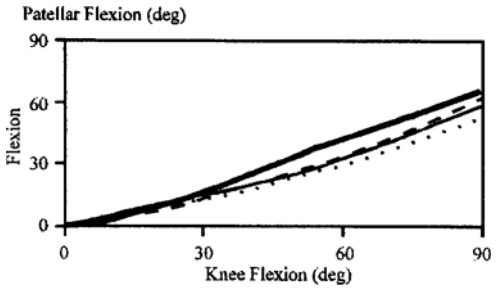

Fig. 14 Comparison of the patellar flexion relative to the femur in the model (heavy solid lines), and in the intact cadaveric knees, for the quadriceps leg raise. The displacements of the patella in the model and in the cadavers were measured relative to the position and orientation of the bone when the knee was placed in full extension (i. e., the reference configuration of the leg). Shown are the measured rotations and translations of the patella relative to the femur for the three specimens tested in Kim (1998).

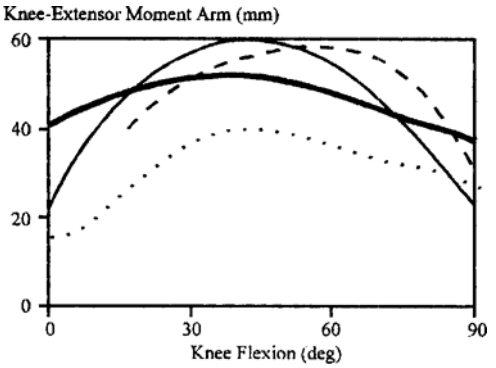

Fig. 15 Comparison of the knee-extensor moment arm for the model (heavy solid line) and those for the cadaveric knees tested in Kim (1998): specimen 1 (solid line), specimen 2 (dashed line), and specimen 3 (dotted line). The knee-extensor moment arm for the model lies within the range calculated for the cadavers at all angles of knee flexion, except near full extension.

However, peak values of these tibial displacements in the model and in the cadavers are small (less than 5 mm).

There is general agreement between the model calculations and measurements of the three-dimensional tracking patterns of the patella for the leg raise task (Fig. 14, compare heavy solid line with light solid, dashed, and dotted lines). The model and the experimental data show that patella flexion lags knee flexion throughout the joint range of motion (Fig. 14, compare heavy solid line with light solid, dashed, and dotted lines). Consistent with experiment, peak values of patellar flexion in the model are around 65°.

6.3 Moment arm of the knee-extensor mechanism

The knee-extensor moment arm calculated for the model lies in the vicinity of those measured for the cadavers (Fig. 15, compare heavy solid line with light solid, dashed, and dotted lines). Consistent with the measurements, the moment arm calculated for the model has a characteristic bell shape when plotted against knee flexion. The knee-extensor moment arm increases as the knee flexes from full extension, peaks at about 35° of flexion, and then decreases rather quickly to a minimum value at 90° of flexion (heavy solid line in Fig. 15). In two of the specimens tested, the knee-extensor moment arms peak at around 40° of flexion, which are close to the value calculated for the model (compare heavy solid line with light solid and dotted lines). For one of the specimens, however, the moment arm peaks at 60° of flexion (dashed line in Fig. 15).

Peak values measured for the knee-extensor moment arms of the cadavers range from 38 cm to 60 cm, with two specimens having similar variations in the shapes and magnitudes of their moment arms. By comparison, the peak value of moment arm in the model is around 50 mm, some 8–10 mm lower than those for the two larger specimens.

It is significant that the moment arm calculated for the model is much higher than those estimated for all the cadavers near full extension of the knee (Fig. 15, compare heavy solid line with light solid, dashed, and dotted lines at 0°). This difference between model and experiment is likely due to differences in the loading applied to the model and the cadavers near full extension of the knee. Near full extension, quadriceps forces applied to extend the cadaveric knees are much greater than

that needed to extend the model knee. Consequently, the perpendicular distance between the screw axis and the line of action of the patellar ligament force in the model remains greater than that in the cadavers (Fig. 15, heavy solid line near full extension). An increase in the applied quadriceps force increases the anterior translation of the tibia relative to the femur, which causes the distance between the screw axis and the line of action of the patellar ligament force to decrease.

Finally, since the loading conditions and constraints applied to the model and the cadavers are similar for most of the range of joint motion, differences between the knee-extensor moment arm calculated for model and those estimated for the cadavers must be due to differences in the geometry of the bones. The fact that the moment arms measured for the three specimens differed by as much as 22 mm, suggests that there is considerable variability in the anatomical dimensions of the specimens alone (Kim, 1998). It is therefore not surprising that a similar level of difference exists between the model and one of the specimens tested, since the model assumes an average shape for each of the bones at the knee.

7. Comparison of Model and Experimental Literature data

In the experiments described in Kim (1998), measurements were made of the applied quadriceps force and the resulting displacements of the bones for three intact knees. Quantitative comparisons between the response of the model and the behavior of a real knee could only be made on the basis of these data (Figs. 12-15). Unfortunately, measurements of knee-ligament and joint-reaction forces could not be obtained from the experiments, so that these quantities could not be compared for the model and the cadavers. However, data for ligament and joint-reaction forces at the knee are available in the literature, though the loading conditions and constraints are different in the various experiments conducted by others. It is useful, nonetheless, to compare, at least qualitatively, the model calculations with these experimental data. A static quadriceps leg raise was simulated using the model. At each angle of knee flexion, a value of quadriceps force was found so that the lower leg remained in static equilibrium. Wherever possible, the resulting ligament and joint-contact forces were then compared with experimental data found in the literature.

7.1 Patellar-ligament and patellofemoral-contact forces

A number of studies have measured the ratio of force in the patellar ligament to the applied force in the quadriceps tendon (Ellis et al, 1980; Buff et al., 1988; Ahmed et al., 1987). In general, the value of this ratio remains near unity from full extension to 30° of flexion, after which it decreases monotonically with increasing knee flexion (Fig. 16). Consistent with the experimental measurements, the model shows that the ratio of patellar ligament force to quadriceps force begins above unity at full extension, increases slightly as the knee flexes to about 20°, and then steadily decreases as knee flexion increases (Fig. 16, compare heavy solid line with solid, dotted, dashed, and dot-dashed lines).

There is also agreement between the model and experimental measurements for the ratio of patellofemoral contact force to applied quadriceps force (Fig. 17). Both the model and the experiments show that the ratio of these forces increase from a value of around 0.5 at full extension to slightly higher than 1.0 at 90° of flexion (compare solid line with dotted line and data points in Fig. 17). The ratio of patellofemoral contact force to quadriceps force is low near full extension because patellofemoral forces are small in this region, irrespective of the magnitude of the applied quadriceps force. Patellofemoral forces are small near full extension because the angle between the patellar ligament and the long axis of the patella remains small. As knee flexion increases, however, patellofemoral forces increase because the angle between the patellar ligament and the long axis of the patella increases. Consequently, the ratio of patellofemoral force to quadriceps force increases.

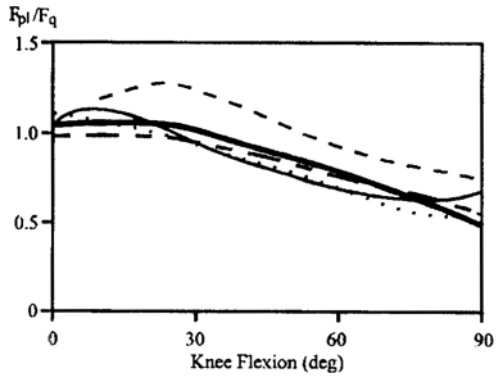

Fig. 16 Ratio of the force developed in the patellar ligament (F_{pl}) to that applied by the quadriceps (F_q) in the model (heavy solid line). The ratio of patellar ligament force to quadriceps force for the model was found by simulating a static quadriceps leg raise task. Experimental data were obtained from the following studies reported in the literature: Buff et al. (1988) (light solid line); Ahmed et al. (1987) (dashed line); Ellis et al. (1980) (dot-dashed line). The dotted line is the results calculated by van Eijden et al. (1986).

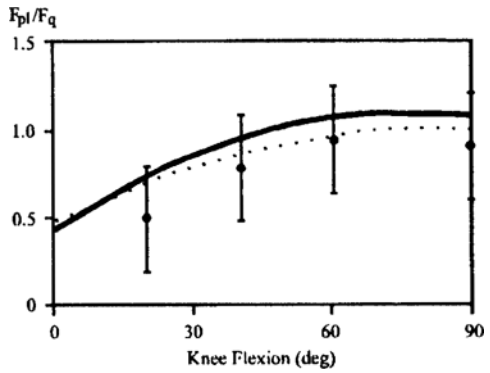

Fig. 17 Ratio of the resultant contact force at the patellofemoral joint (F_{pf}) to the applied quadriceps force (F_q) in the model (heavy solid line). The ratio of patellofemoral contact force to quadriceps force for the model was found by simulating a static quadriceps leg raise task. The dotted line is the result calculated by van Eijden et al. (1986) using a two-dimensional model of the patellofemoral joint. Data points correspond to measurements reported by Ahmed et al. (1987) (●).

7.2 Ligament forces

The model ACL is loaded near full extension during a quadriceps leg raise; the model PCL remains slack (Fig. 18, aAC, pAC, aPC, and pPC). This is consistent with experimental data provided by Markolf et al. (1990), who measured forces in the whole ACL during slow extension of the intact knee (Fig. 18, add aAC and pAC and compare with filled diamonds). Total ACL force near extension is higher in the model than in the cadavers because a constant 200 N pull was applied to the quadriceps tendon in the experiments, whereas 280 N of quadriceps force is required to equilibrate the model leg at full extension. In contrast to the behavior of the ACL, the model PCL begins to bear load only at 55° of flexion, and the force in this ligament increases with increasing knee flexion (Fig. 18, aPC and pPC). There is at least qualitative agreement between these results and the measurements reported by Wascher et al. (1993) (c. f. aPC and pPC with filled circles in Fig. 18). Notice, however,

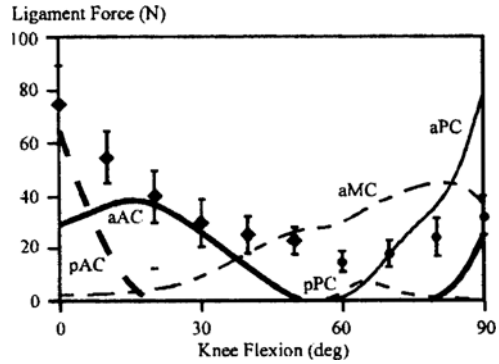

Fig. 18 Cruciate and collateral ligament forces calculated for the model (aAC, heavy solid line; pAC, heavy dashed line; aPC, light solid line; pPC, light dashed line); aMC, dot-dashed line). Resultant forces in the model ACL and model PCL are higher at full extension and at 90° of flexion, respectively. Experimental data for the resultant forces in the ACL (◆) and PCL (●) were obtained from Markolf et al. (1990) and Wascher et al. (1993), respectively. Forces induced in the various bundles of MCL, LCL, and capsule were all much smaller than those shown for the cruciate ligaments.

that the model PCL is more heavily loaded than the real ligament at 90° of flexion (Fig. 18, light solid line at 90°).

The force borne by the model MCL increases as knee flexion angle increases (Fig. 18, aMC). Only the model aMC bears force during the quadriceps leg raise task; the force in each of the remaining bundles of the model MCL remain zero throughout the range of knee flexion. The forces borne by the LCL and each of the separate bundles of the posterior capsule in the model are also zero for the duration of the leg raise task. These results suggest that only the model aMC is recruited as the knee rotates internally during flexion.

7.3 Shear forces at the knee during a quadriceps leg raise

During static quadriceps leg raise, the tibia was statically equilibrated in the anterior and posterior direction by shear forces of twelve ligaments and the resultant shear force from the tibiofemotal contact, patellar ligament, and leg weight. Figure 19 shows the shear components of forces applied to the tibia. The shear force of the tibiofemoral contact, which is applied anteriorly to the tibia, increases as the knee extends because the force of the patellar ligament increases. The shear force of the patellar ligament also increases because both the orientation of this ligament relative to the long axis of the tibia and the magnitude of the patellar ligament force which results from an increase in quadriceps force increase. The model ACL is posteriorly loaded for all flexions except the range of 60 ° to 80 °; the MCL is also posteriorly loaded from 10° to 90°; the PCL is anteriorly loaded beyond 80° of flexion:

The overall pattern of cruciate ligament loading is explained by the variation in the resultant shear force applied to the tibia (Fig. 19). The model ACL is loaded from 60° to full extension because the resultant shear force is directed anteriorly; the PCL is loaded beyond 80° of flexion as the total shear force, the ACL, and the MCL then acts posteriorly (Fig. 19, compare ACL and PCL with Total). The resultant shear force applied to the tibia is dominated by the action of the patellar ligament (Figs. 18 and 19, PL).

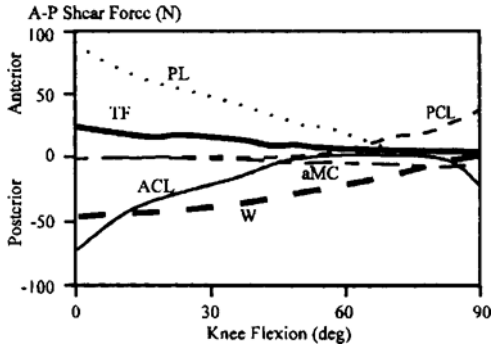

Fig. 19 Anterior-posterior shear forces applied to the model tibia for the quadriceps leg raise task. Patellar ligament shear force, PL (dotted line); tibiofemoral contact shear force, TF (heavy solid line); shear force due to the leg weight, W (heavy dashed line); resultant shear force due to the anterior cruciate ligament, ACL (light solid line); resultant shear force due to the posterior cruciate ligament, PCL (light dashed line). resultant shear force due to the anterior bundle of the MCL, aMC (dot-dashed line). The PL, TF, and PCL are apply anteriorly-directed shear forces to the tibia; The ACL, MCL and leg weight all apply posteriorly-directed shear forces to the tibia. Adding all the curves shown in the graph together will give zero, indicating that the tibia is in static equilibrium in the anterior-posterior direction.

8. Limitations of the Model

We have introduced a number of simplifications into the kinematical structure of our model for the knee-extensor mechanism. Perhaps most significantly, we approximated the tibial plateau and patellar facet as flat surfaces. In view of the shapes of parasagittal sections taken through the tibia and patella, these approximations appear to be reasonable, at least in the range 0°-90° of flexion. As the knee flexes beyond 90 deg, however, the validity of our model is brought into question, as the patellar facet no longer contacts the femur in the region of the femoral groove. Instead, patellofemoral contact resides on portions of the medial and lateral femoral condyles

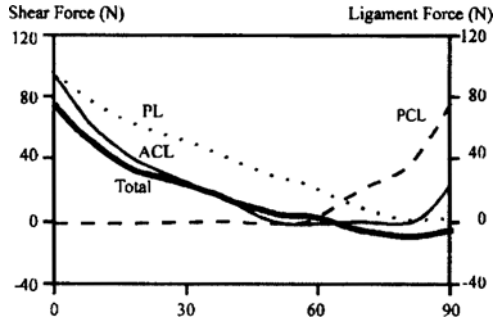

Fig. 20 Interaction between tibiofemoral ligaments and a patellar ligament: PL (dotted line) is the shear force supplied by the patellar ligament. Total (heavy solid line) represents the resultant shear force applied to the tibia by the tibiofemoral contact (TF), the patellar ligament (PL), and the leg weight (W). The resultant force of the anterior cruciate ligament for the static quadriceps leg raise is represented as ACL (light solid line) and the resultant force of the posterior cruciate ligament as PCL (dashed line). The difference between Total and PL represents the contributions from the tibiofemoral contact force and the leg weight applied to the tibia. Notice that the total force in the model ACL (light solid line) is higher than the resultant anterior drawer (Total, heavy solid line). This is consistent with experimental data which show that the load on the whole ACL can exceed the magnitude of the applied anterior drawer by as much as 30 percent (Markolf et al., 1990). At small angles of the knee, each bundle of the model ACL is inclined at an angle of about 25° to the long axis of the tibia. Total ACL force therefore exceeds the applied anterior drawer by a function of the cosine of this angle.

(Ahmed et al., 1983). Since our model fails to account for these effects, its applicability is limited to the range 0°-90° of flexion.

Acknowledgments

The author would like to express his appreciation to Dr. Marcus Pandy and the Biomechanics Laboratory of The University of Texas at Austin for their assistance in this study.

References

Ahmed, A. M., Hyder, A., Burke, D. L., and Chan, K. H., 1987, "In-vitro Ligament Tension Pattern in the Flexed Knee in Passive Loading," *J. Orthop. Res.*, Vol. 5, pp. 217~230.

Ahmed, A. M., Burke, D. L., and Yu, A., 1983, "In-vitro Measurement of Static Pressure Distribution in Synovial Joints- Part II: Retropatellar Surface," *J. Biomech. Engng.*, Vol. 105, pp. 226~236.

Andriacchi, T. P., Mikosz, R. P., Hampton, S. J., and Galante, J. O., 1983, "Model Studies of the Stiffness Characteristics of the Human Knee Joint," *J. Biomechanics,* Vol. 16, pp. 23~29.

Blankevoort, L., Kuiper, J. H., Huikes, R., Grootenber, H. J., 1991, "Articular Contact in a Three-Dimensional Model of the Knee," *J. of Biomechanics,* Vol. 24, pp. 1019~1031.

Blankevoort, L., Huikes, R., and de Lange, A., 1988, "The Envelop of Passive Knee Joint Motion," *J. of Biomechanics,* Vol. 24, pp. 1019~1031.

Buff, H. U., Jones, L. C., and Hungerford, D. S., 1988, "Experimental Determination of Force Transmitted Through the Patello-Femoral Joint," *J. Biomechanics,* Vol. 21, pp. 17~23.

Butler, D. L., Kay, M. D., and Stouffer, D. C., 1986, "Comparison of Material Properties in Fascicle-Bone Units From Human Patellar Tendon and Knee Ligaments," *J. Biomechanics,* Vol. 19, pp. 425~432.

Butler, D. L., Noyes, F. R., Grood, E. S., 1980, "Ligamentous Restraints to Anterior-Posterior Drawer in the Human Knee," *J. Bone Jt. Surg.,* Vol. 62-A, pp. 259~270.

Dowson, D. and Jin, Z., 1990, "The Influence of Elastic Deformation Upon Film Thickness in Lubricated Bearings With Low Elastic Modulus Coatings," Mechanics of Coatings, Tribology series 17. Elsevier Science Publishing Co. Proceedings of the 16th Leeds-Lyon symposium on tribology. 5th-8th Sept. 1989. (eds.) In Dowson, D. et al. pp. 263~269.

Dowson, D. and Taylor, C. M., 1967, "Elasto-hydrostatic Lubrication of Circular Plate Thrust

Bearings," *J. Lubrication Technology, ASME.* pp. 244~237.

Ellis, M. I., Seedom, B. B., Wright, V., and Dawson, C. E., 1980, "An Evaluation of the Ratio Between the Tensions Along the Quadriceps Tendon and the Patella Ligament," *Engng. Med.,* Vol. 9, pp. 189~194.

Essinger, J. R., Leyvraz, P. F., Heegard, J. H., Robertson, D. D., 1989, "A Mathematical model for the Evaluation of the Behavior During Flexion of Condylar-Type Knee Prothesis," *J. of Biomechanics,* Vol. 22, pp. 1229~1241.

Foley, J. D. and van Dam A., 1982, "Fundamentals of Interactive Computer Graphics", Addison-Wesley Pub.

Fukubayashi, T., Torzilli, P. A., Sherman, M. F., and Warren R. F., 1982, "An in Vitro Biomechanical Evaluation of Anterior-Posterior Motion of the Knee," *J. Bone Jt. Surg.,* Vol. 64 -A, pp. 258~264.

Garg, A. and Walker, P. S., 1990, "Prediction of Total Knee Motion Using a Three-Dimensional Computer-Graphic Model," *J. Biomechanics,* Vol. 23, pp45~50.

Girgis, F. G., Marshall, J. L., and AlMonajem, A. R. S., 1975, "The Cruciate Ligaments of the Knee Joint," *Clin. Orthop. Scan.,* Vol. 51, pp. 136 ~144.

Hayes, W. C. and Bodine, A. J., 1978, "Flow -Independent Viscoelastic Properties of Articular Cartilage," *J. Biomechanics,* Vol. 11, pp. 407 ~419.

Heegard, J., Leyvraz, P. F., Curnier, A., Rakotomanana, L. and Huiskes, R., 1995, "The Biomechanics of the Human Patella During Passive Knee Flexion," *J. Biomechanics,* Vol. 28, pp. 1265~1279.

Hefzy, M. S. and Yang, H., 1993, "A Three -Dimensional Anatomical Model of the Human Patellofemoral Joint for the Determination of Patellofemoral Motions and Contact Characteristics," *J. Biomedical Engng,* Vol. 15, pp. 289 ~302.

Hirokawa, S., 1991, "Three-Dimensional Mathematical Model Analysis of the Patellofemoral Joint," *J. Biomechanics,* Vol. 24, pp. 659~671.

Hori, R. Y. and Mockros, L. F., 1976, "Indention Tests of Human Articular Cartilage," *J. Appl. Physiol.,* Vol. 31, pp. 562~568.

Johnson, K. L., 1985, Contact Mecahnics. Cambridge University Press. Chapter 4 and 5. pp. 85~152.

Kim, S., 1998, "In-vitro Measurement of the Human Knee Joint Motion During Quadriceps Leg Raising," KSME International Journal, Vol. 12, No. 4, pp. 624~641.

Kim, S., 1996, "A three-dimensional Dynamic Musculoskeletal Model of the Human Knee Joint," Ph. D. Dissertation, Mechanical Engineering Dept. The University of Texas at Austin, TX, U. S. A

Koh, T. J., Grabiner, M. D., and De Swart, R. J., 1992, "In Vivo Tracking of the Human Patella," *J. Biomechanics,* Vol. 25, pp. 637~643.

Kurosawa, H., Walker, P. S., Abe, S., Garg, A., and Hunter, T., 1985, "Geometry and Motion of the Knee for Implant and Orthotic Design," *J. Biomechanics.* Vol. 18, pp. 487~499.

Mak, A. F., 1986, "The Apparent Viscoealstic Behavior of Articular Cartilage: the Contributions from the Intrinsic Matrix Viscoelasticity and Interstitial Fluid Flow," *J. Biomech. Engng.,* Vol. 108, pp. 123~130.

Markolf, K. L., Gorek, J. F., Kabo, M. et al., 1990, "Direct Measurement of Resultant Forces in the Anterior Cruciate Ligament," *J. of Bone Jt. Surg.,* Vol. 72-A, pp. 557~567.

Markolf, K. L., Bargar, W. L., Shoemaker, S. C. et al., 1981, "The Role of Joint Load in Knee Stability," *J. Bone Jt. Surg.,* Vol. 63-A, pp. 570 ~585.

Markolf, K. L., Mensch, J. S., Amstutz, H. C. et al., 1976, "Stiffness and Laxity of the Knee: The Contributions of the Supporting Structures," *J Bone Jt. Surg.,* Vol. 58-A, pp. 583~593.

Nielsen, S., Ovesen, J. and Andersen, K., 1984, "Rotary Instability of Cadaver Knees After Transection of Collateral Ligaments and Capsule," *Arch. Orthop. Traum. Surg.,* Vol. 103, pp. 165 ~169.

Nisell, R, 1985, "Mechanics of the knee." *Acta Orthop. Scand.* Supplementum 216, Vol. 56, pp. 1 ~42.

Norwood, L. A. and Cross, M. J., 1977, "The Intercondylar Shelf and the Anterior Cruciate Ligament," *Am. J. Sports Med.,* Vol. 5, pp. 171 ~176.

O'Connor, J. J., Biden, E., Bradley, J., Fitzpatrick, D., Young, S., Kershaw, C., Daniel, D., and Goodfellow, J., 1990, "The Muscle-Stabilized Knee," In Daniel, D., Akeson, W., and O' Connor, J. (eds.): Knee Ligament: Structure, Function, and Repair. Raven Press, New York, pp. 239~277.

Pizali, R. L., Seering, W., Nagel, D. A. and Schurman, D. J., 1980, "The Function of the Primary Ligaments of the Knee in Anterior-Posterior and Medial-Lateral Motions," *J. Biomechanics,* Vol. 13, pp. 777~784.

Reicher, M. A., 1993, "An Atlas of Normal Multiplanar Anatomy of the Knee Joint," In Mink, J. H., Reicher, M. A., Crues, J. V., and Deutsch, A. L. (eds): MRI of the knee, Raven Press, New York, pp. 51~90.

Reuben, J. D., Rovick, J. S., Schrager, R. J., Walker, P. S., and Boland, A. L., 1989, "Three -dimensional Dynamic Motion Analysis of the Anterior Cruciate Ligament Deficient Knee Joint," *Amer. J. Sports Med.,* Vol. 17, pp. 463 ~471.

Shoemaker, S. C., and Markolf, K. L., 1985, "Effects of Joint Load on the Stiffness and Laxity of Ligament-Deficient Knees," *J. Bone Jt. Surg.,* Vol. 67-A, pp. 136~146.

Smidt G. L., 1973, "Biomechanical Analysis of Knee Flexion and Extension," *J. of Biomechanics,* Vol. 6, pp. 79~92.

Symbolic Dynamics Inc., 1992, SD/Fast User's Manual, Sunnyvale, California. U. S. A.

Tumer S. T. and Engin A. E. (1993). Three -body Segment Dynamic Model of the Human Knee. *J. Biomech. Engng.* 115: 357-365.

van Eijden, T. M., Kouwenhoven, E., Verburg, J., and Weijs, W. A., 1986, "A Mathematical Model of the Patellofemoral Joint," *J. Biomechanics,* Vol. 19, pp. 219~229.

Wascher, D. C., Markolf, K. L., Shapiro, M. S., and Finerman, G. A., 1993, "Direct in Vitro Measurement of Forces in the Cruciate Ligaments. Part1: The Effect of Multiplane Loading in the Intact Knee," *J. Bone Jt. Surg.,* Vol. 75-A, pp. 377~386.

Wu, G. and Cavanagh, P. R., 1995, "ISB Recommendations for Standardization in the Reporting of Kinematic Data," *J. Biomechanics,* Vol. 28, pp. 1257~1261.

Yamaguchi, G. T. and Zajac, F. E., 1989, "A Planar Model of the Knee Joint to Characterize the Knee Extensor Mechanism," *J. Biomechanics,* Vol. 22, pp. 1~10.